Astron. Astrophys. 72, 348–355 (1979)

ASTRONOMY AND ASTROPHYSICS

Non-linear Dynamo Theory: Finite Amplitude Magnetic Fields with Large Scale Circulation in a Compressible Stratified Medium

M. Schüßler

Universitäts-Sternwarte, Geismarlandstr. 11, D-3400 Göttingen, Federal Republic of Germany

Received May 11, revised June 20, 1978

Summary. In the framework of dynamo theory of the solar cycle self-consistent numerical solutions of the non-linear mean field MHD equations (including Lorentz force) within a compressible stratified medium are given for a cartesian geometry. For both steady (α^2) and oscillatory ($\alpha\omega$) turbulent dynamos the growth of the magnetic field is limited by a mean flow driven by the Lorentz force. Magnetic buoyancy supports this mechanism but is not able to suppress dynamo action totally or to set narrow limits to the dynamo models investigated. Flow velocities of the order of 1 m s^{-1} are sufficient to limit the magnetic field amplitude to about 10 mT (mean toroidal field of the Sun). For an oscillatory dynamo of the solar type the flow pattern has a one-cell-geometry with fluid rising to the surface near the spot zone (zone of maximum toroidal field in the vicinity of the equator), flowing towards the pole and sinking down there. This may account for the observed poleward motion of the prominence zone.

Key words: α-effect – dynamo – hydromagnetics – magnetic field – solar cycle

1. Introduction

The concept of mean field electrodynamics (recently reviewed by Krause, 1976; see also Moffat, 1978) led to the construction of turbulent α-effect dynamo models for the solar cycle (recently reviewed by Stix, 1976a), the Earth's magnetic field (Steenbeck and Krause, 1969; Deinzer et al., 1974), magnetic fields in pre-main-sequence evolution and Ap-stars (Schüßler, 1975), fields in the convective cores of massive stars (Pähler, 1976) and the galactic field (Stix, 1975). All these investigations used either the pure kinematic approach, i.e. no reaction of the growing magnetic field on the motions driving the dynamo was taken into account (therefore an exponential growth of the field resulted) or used a very crude model, the "cut-off-α-effect" (Stix, 1972; Jepps, 1975), in order to produce a finite amplitude magnetic field. Cut-off-α-effect means that the induction term (i.e. α) is arbitrarily set zero if the magnetic field exceeds some critical value, B_c, generally identified with the equipartition value with respect to the fluid motion (but see Busse, 1975; Galloway et al., 1977; Peckover and Weiss, 1978). Other ad-hoc models for a non-linearity were given by Rüdiger (1973) and Yoshimura (1978a, b). In the framework of his dynamo model, Moffat (1972) gave a consistent description of the reaction of the magnetic field on the induction mechanism. Recently, Watanabe (1977) calculated the depence of α on the field strength and applied the results to a turbulent dynamo in the Earth's core. Another approach to nonlinear effects in the small scale is due to Vainshtein (1971). Frisch et al. (1975; see also Pouquet and Patterson, 1978) paid attention to inverse cascades of magnetic helicity towards small wavenumbers in turbulent media including dynamical effects.

Rather than looking at the field regeneration mechanism in the small length scale, Malkus and Proctor (1975) investigated the capability of large scale motions driven by the mean magnetic field through the Lorentz force to limit the magnetic field to a finite amplitude. For an incompressible medium it was possible to construct such models by means of numerical integration for α^2-dynamos (Proctor, 1977; Hellmich, 1978) and $\alpha\omega$-dynamos (Nelle, 1977). This field limitation process resembles that used by Busse (1973) in the framework of his dynamo model. Other hydromagnetic dynamo models were constructed by Soward (1973) and Gubbins (1975). The investigations referred to above dealt with incompressible or Boussineq media. However, calculations for the compressible case with a strongly stratified medium are necessary to reach a better approximation to the situation in the convective regions of stars and the Sun.

Parker (1977) claimed that "*buoyancy has important quantitative effects on the operation of the solar dynamo*". This conclusion was drawn from an estimate of the rising velocity of individual flux tubes (Parker, 1975). However, inclusion of the effects of tube expansion and viscosity reduces the rising velocity drastically (Schüßler, 1977) and from this point of view there seem to be no severe restrictions to the operation of the solar dynamo. On the other hand, the influence of buoyancy on the mean field dynamo process can be investigated consistently only by a MHD calculation including the buoyancy term in the momentum equation for a compressible medium stratified by a gravitational acceleration. Together with the information about the effect of buoyancy we then gain insight into the pattern of flow associated with large scale dynamo action, especially for the case of the Sun.

2. Equations and Procedure

Consider a cartesian coordinate system (x, y, z). We shall solve the MHD equations within the rectangular domain $0 \leqq x \leqq L$, $0 \leqq z \leqq L$ with a length scale L, assuming infinite extension in y-direction with $\partial/\partial y = 0$. The equations that describe the problem are

$$\rho\left[\frac{\partial \mathbf{u}}{\partial t} + (\mathbf{u}\cdot\nabla)\mathbf{u}\right] = -\nabla p + \frac{1}{4\pi}(\nabla\times\mathbf{B})\times\mathbf{B} + \rho\mathbf{g} + \nu[\nabla^2\mathbf{u} + \tfrac{1}{3}\nabla(\nabla\cdot\mathbf{u})]\,. \quad (1)$$

$$\frac{\partial \rho}{\partial t}+\nabla\cdot(\rho\mathbf{u})=0. \tag{2}$$

$$\frac{\partial \mathbf{B}}{\partial t}=\nabla\times(\mathbf{u}\times\mathbf{B}+\alpha\mathbf{B})+\eta\nabla^2\mathbf{B}. \tag{3}$$

$\mathbf{B}=(B_x,B_y,B_z)$ denotes the mean magnetic field, $\mathbf{u}=(u_x,u_y,u_z)$ the mean velocity, ρ the mass density, p the gas pressure, α the turbulent induction (α-effect); all variables quoted so far are functions of x, z and t. $\mathbf{g}=(0,0,-g)$ denotes the constant gravitational acceleration, ν the dynamical viscosity and η the magnetic diffusivity. Equation (1) is the momentum equation, Eq. (2) the equation of continuity and Eq. (3) the MHD induction equation. To close this set we assume the ideal gas law with a temperature profile $T(z)$ which does not vary in time. Hence, we do not include an energy equation; this is possible because the presence of a weak magnetic field (say, 10 mT mean toroidal field for the solar convection zone) does not have a significant influence on the (convective or radiative) energy transport and the temperature profile. However, this assumption may not be justified for concentrated ($\gtrsim$1 T) rather than mean fields, but such flux concentrations are not included in the theory presented here.

Locally, i.e. for regions small enough for curvature to be unimportant, we can identity (x,y,z) with spherical polar coordinates (ϑ,φ,r) and the condition $\partial/\partial y=0$ with axisymmetry, $\partial/\partial\varphi=0$. In the case of the Sun this is possible if we use $L=2\,10^8$ m, the vertical extension of the convection zone (Baker and Temesváry, 1966). The rectangular region has the topology of a spherical shell with the depth of the convection zone ($z=0$: bottom, $z=L$: surface) and a horizontal extension from pole ($x=0$) to equator ($x=L$). Therefore, we can speak of a "toroidal" magnetic field $\mathbf{B}_t=(0,B_y,0)$ and a "poloidal" field $\mathbf{B}_p=(B_x,0,B_z)$ and define $\mathbf{u}_p$ and $\mathbf{u}_t$ analogously. Let us rewrite Eqs. (1)–(3) in a more suitable form by introduction of the following modifications:

a) Subtraction of the undisturbed hydrostatic stratification $p_H(z)$, $\rho_H(z)$ with $dp_H/dz=-\rho_H\cdot g$ from the momentum Eq. (1)

b) Introduction of a vector potential $\mathbf{A}=(0,A_y,0)$ for the poloidal field with $\mathbf{B}_p=\nabla\times\mathbf{A}$ in order to omit one equation and satisfy $\nabla\cdot\mathbf{B}=0$ automatically

c) Usage of dimensionless variables

d) Inclusion of an arbitrary additional toroidal shear flow $\mathbf{u}_s(z)=(0,u_s(z),0)$ assumed not to be influenced by the magnetic field. u_s resembles a differential rotation and is needed to calculate $\alpha\omega$-dynamos.

This procedure results in the following set of dimensionless equations (for simplicity we use the same symbols for the dimensionless variables as before).

$$\rho\left[\frac{\partial\mathbf{u}}{\partial t}+(\mathbf{u}\cdot\nabla)\mathbf{u}\right]=-\Gamma(G^{-1}\nabla\tilde{\rho}T+\tilde{\rho}\hat{\mathbf{z}})+(\nabla\times\mathbf{B})\times\mathbf{B}+P_m(\nabla^2\mathbf{u}+\tfrac{1}{3}\nabla(\nabla\cdot\mathbf{u})) \tag{4}$$

$$\frac{\partial\tilde{\rho}}{\partial t}=-\nabla\cdot(\rho\mathbf{u}). \tag{5}$$

$$\frac{\partial\mathbf{B}_t}{\partial t}=(\mathbf{B}_p\cdot\nabla)\mathbf{u}_s+\nabla\times(\mathbf{u}_t\times\mathbf{B}_p+\mathbf{u}_p\times\mathbf{B}_t)+R_\alpha\nabla\times(\hat{\alpha}\cdot\mathbf{B}_p)+\nabla^2\mathbf{B}_t \tag{6}$$

$$\frac{\partial\mathbf{A}}{\partial t}=(\mathbf{u}_p\times\mathbf{B}_p)+R_\alpha\cdot\hat{\alpha}\cdot\mathbf{B}_t+\nabla^2\mathbf{A}.$$

$\tilde{\rho}$ is the density perturbation (total density minus hydrostatic density). Since (5) is a scalar equation and only the y-components of (6) and (7) do not vanish, this represents a system of 6 equations for 6 variables $\mathbf{u},\tilde{\rho},B_y,A_y$. The dimensionless numbers that describe the physical situation are:

$$\Gamma=g\cdot L^3\cdot\eta^{-2}, \tag{8}$$

the non-dimensional gravity,

$$G=L\cdot\Lambda^{-1}, \tag{9}$$

the number of isothermal scale heights $\Lambda=\mathscr{R}T_0/\mu g$ in the box, where T_0 is the temperature scale and $\mathscr{R}$ is the universal gas constant,

$$P_m=\nu\cdot(\rho_0\eta)^{-1}, \tag{10}$$

the magnetic Prandtl number, where $\rho_0=\rho_H(0)$ is the scale of the density,

$$R_\alpha=\alpha_0\cdot L\cdot\eta^{-1}, \tag{11}$$

the α-Reynolds number with α_0, the scale of the α-effect. The function $\hat{\alpha}$ in Eqs. (6) and (7) represents the spatial dependence of the α-effect (i.e. $\hat{\alpha}$ is a normalized profile). When $u_s\neq0$ there is a fifth prescribed parameter

$$R_\omega=k_0\cdot L\cdot\eta^{-1}, \tag{12}$$

the 'shear' Reynolds number, where k_0 is a typical velocity difference which will be specified later.

In the case of P_m we have to distinguish between non-turbulent and turbulent media. For the former, the dynamical viscosity ν is constant (independent of density, $P_m=$const.) while within a turbulent medium (as the solar convection zone seems to be), the kinematical viscosity $\nu/\rho\sim v_t\cdot l$ ($v_t=$turbulent velocity, $l=$typical extension of a turbulent eddy) is constant (i.e. $P_m\sim\rho$). We show results for both cases in the next section; they are slightly different. As time unit in Eqs. (4)–(7) we use the magnetic diffusion time $\tau_D=L^2\eta^{-1}$ while the velocity scale is $u_0=\eta\cdot L^{-1}$. The scale B_0 of the magnetic field is chosen such as to give

$$B_0^2\cdot L^2/(4\pi\cdot\rho_H(0)\cdot\eta^2)=V_{A,0}^2/U_0^2=1, \tag{13}$$

where $V_{A,0}$ is the Alfvén velocity relevant for B_0 and $\rho_0=\rho_H(0)$. As boundary conditions we assume $A_y=B_y=0$ for all boundaries, thus limiting the magnetic field to the integration domain. Consequently, the Lorentz force vanishes at the boundaries and it is consistent to use free slip boundaries for the fluid motion, i.e. vanishing normal component of the velocity and vanishing normal derivative of the tangential component at the boundaries. Together we have:

$$A_y=B_y=u_z=\partial u_x/\partial z=\partial u_y/\partial z=0 \quad \text{for} \quad z=0, \quad z=1. \tag{14}$$

$$A_y=B_y=u_x=\partial u_z/\partial x=\partial u_y/\partial x=0 \quad \text{for} \quad x=0, \quad x=1. \tag{15}$$

Equations (4)–(7) together with the boundary conditions (14) and (15) have been solved numerically as an initial value problem using the explicit finite difference scheme of Dufort and Frankel (1953). Stability problems arising in the course of test calculations made it necessary to include an arbitrary diffusion term in the equation of continuity (5) (Harlow and Amsden, 1971) which then reads

$$\frac{\partial\tilde{\rho}}{\partial t}=-\nabla\cdot(\rho\mathbf{u})+\gamma\nabla^2\rho. \tag{5'}$$

The parameter γ can be adjusted for numerical convenience. We use $\gamma=0.5$ throughout the calculations. The dependence of the results on γ is negligible; this was tested by variation of γ in the range $0.25\leqq\gamma\leqq1$. (5′) is of second order and we have to add another boundary condition. We assume a vanishing normal deriv-

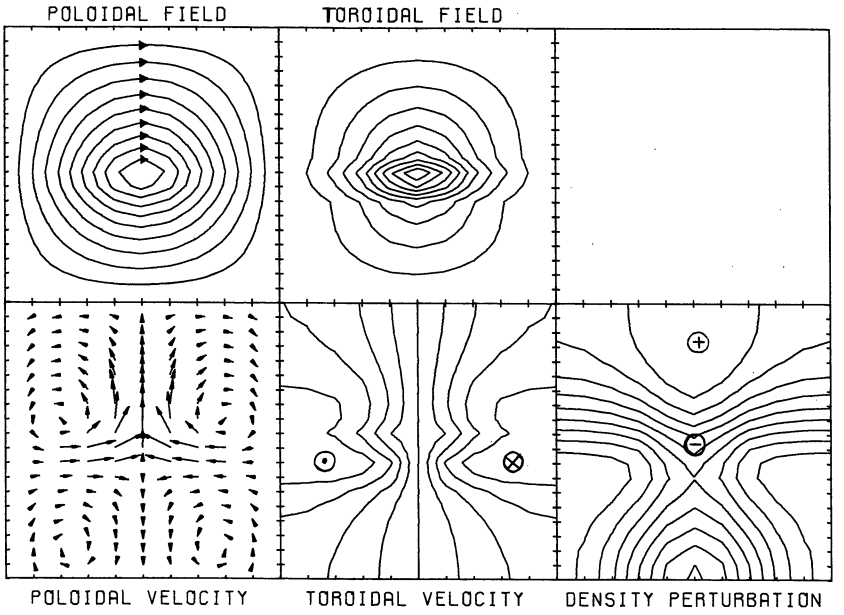

Fig. 1. Stationary configuration of magnetic field, flow pattern and density perturbation for an α^2-dynamo with 4 scale heights for the turbulent case

ative:

$$\begin{aligned} \partial\rho/\partial x &= 0 \quad \text{for} \quad x=0, \quad x=1 \\ \partial\rho/\partial z &= 0 \quad \text{for} \quad z=0, \quad z=1. \end{aligned} \tag{16}$$

Through this choice we avoid mass diffusion across the boundaries and ensure constant mass within the integration domain.

3. Results

Parameter Choice

A simple model ($\mathbf{u}\equiv\mathbf{0}$, $\alpha=$const.) which can be easily solved analytically has been used to test the numerical method and to choose optimal values for timestep Δt and grid dimensions. $\Delta t = 10^{-3}$ and a grid with 11 points in x-direction and 20 points in z-direction resulted as the best choice and these values have been used throughout the calculations.

The dimensionless numbers Γ, G, P_m, R_α have been determined by our aim to apply the calculations primarily to the solar convection zone; however, the results are relevant in principle for all astrophysical situations where an active turbulent dynamo is possible. With $L=2\ 10^8$ m and a turbulent magnetic diffusivity $\eta=10^8$ m^2 s^{-1} (Köhler, 1973) the velocity scale is $u_0=0.5$ m s^{-1}. A gravitational acceleration $g=2.7\ 10^2$ m s^{-2} leads to $\Gamma\approx 2\ 10^{11}$ for the case of the Sun. This value is much too big to be tolerated by the numerical scheme. However, only the value of $G=L\cdot\Lambda^{-1}$ determines the effect of buoyancy (Schüßler, 1978), i.e. only the ratio of the factors in front of gravity and pressure in the momentum Eq. (4). With a typical value of 10^6 K for the lower convection zone we get $G\approx 6$. We use values in the range $G=0\ldots 5$ and $\Gamma=100$. Still $\Gamma\gg 1$ holds and the main properties of the results are likely to be relevant for the Sun. Using $\rho_0=10^{-2}$ g cm^{-3} condition $V_{A,0}/u_0=1$ gives $B_0=1.8$ mT for the scale of the magnetic field. The magnetic Prandtl number P_m characterizes the efficiency of viscous compared to Ohmic dissipation. As mentioned in the preceding section we have to distinguish between the laminar case ($P_m=$const.) and the turbulent case [$P_m=P_m(z=0)\cdot\rho(z)$]. We shall show results for both cases in the range $P_m=0.02\ldots 1.0$; the upper value seems to be plausible for fully developed turbulence.

Isothermal Model: α^2-dynamo

In order to demonstrate the principal properties of the solutions we choose an isothermal situation as a simple model which preserves the main features. It has the advantage of a constant scale height of pressure and density. The interesting features, i.e. the geometry of magnetic field and flow pattern and the influence of buoyancy and compressibility on the field limitation can be clarified with this model; the inclusion of a temperature stratification leads only to small quantitative changes.

First we show results for an α^2-dynamo, a dynamo operating only through turbulent induction (α-effect). In order to investigate the influence of buoyancy we restrict the induction region to a small horizontal strip $z_1 \lesssim z \lesssim z_2$, using the error function Φ for a smooth transition (Roberts and Stix, 1972):

$$\hat{\alpha}(z)=0.5\cdot\left[\Phi\left(\frac{z-z_1}{d}\right)-\Phi\left(\frac{z-z_2}{d}\right)\right], \tag{17}$$

d is the width of the transition zone; a small value of d (e.g. $d=0.05$) restricts the α-effect almost completely to the interval $[z_1, z_2]$. Buoyancy tends to transport magnetic flux out of this region and therefore supports field limitation. We shall show, however, that buoyancy is not able to stop dynamo action completely if we use a reasonable number of scale heights. Stationary field configurations and the flow pattern for a model with $z_1=0.4$, $z_2=0.5$, and $\Gamma=100.0$, $G=4$ are shown in Fig. 1 for the case of constant (turbulent) kinematic viscosity with $P_m(0)=1$. Calculations without velocity field show that the dynamo is excited for $R_\alpha \gtrsim 19.25$; we use $R_\alpha=20.5$ to be well beyond the critical value. A stationary state is reached within 2 or 3 magnetic diffusion times; it does not depend on the choice of the initial values. We use

$$\mathbf{u}=\mathbf{0},\ B_y^{(0)}=A_y^{(0)}=c_0\cdot\sin(\pi\cdot x)\cdot\sin(\pi\cdot z) \quad \text{for} \quad t=0.$$

For $c_0=0.01$ we have an initial toroidal field of 0.02 mT maximum. $B_y^{(0)}$ and $A_y^{(0)}$ are 'seed fields' which are amplified through

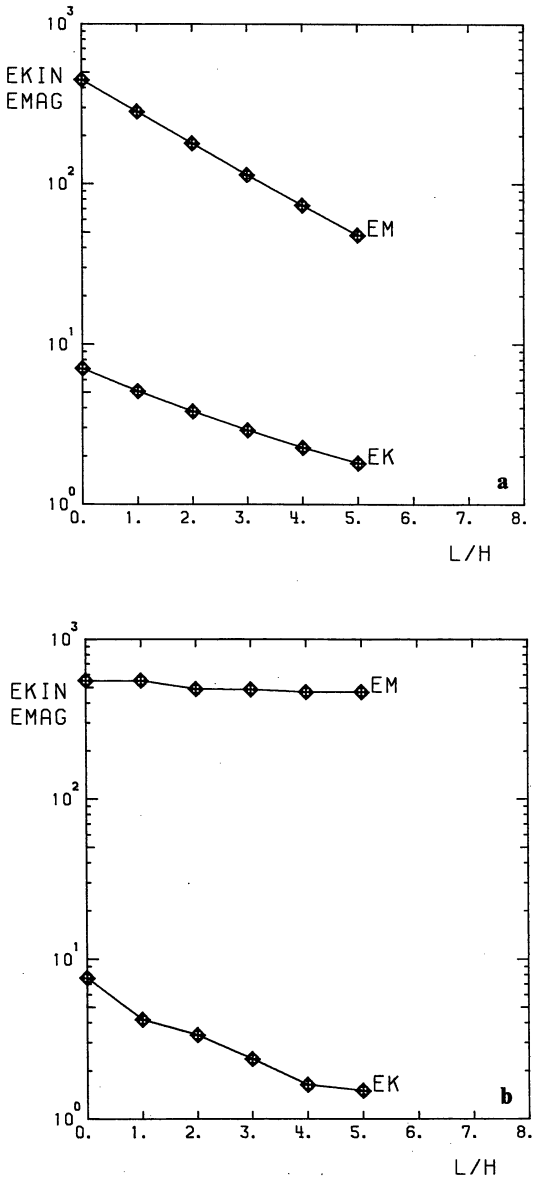

Fig. 2. a Kinetic and magnetic energy (per unit length, arbitrary units) as functions of the number of scale heights within the integration domain. Rhombs indicate the values calculated. (Turbulent case) **b** Same as Fig. 2a for the non-turbulent case

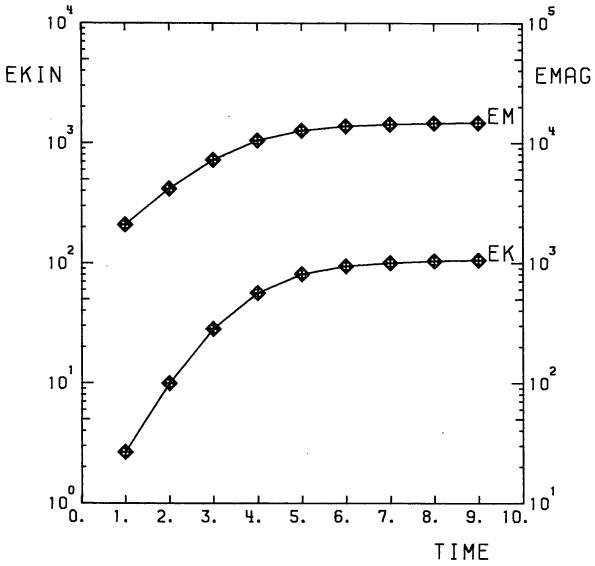

Fig. 3. Time evolution of E_{kin} and E_{mag} (per unit length, arbitrary units) for the model of Fig. 1 with $R_\alpha = 19.5$. Time is given in units of the magnetic diffusion time. Note the different scales for E_{kin} and E_{mag}. Rhombs indicate the values calculated. (Turbulent case)

dynamo action. Each frame in Fig. 1 represents the integration domain. The grid resolution is indicated by small bars. The left frame in the upper row shows field lines of the poloidal field $(B_x, 0, B_z)$, the middle frame contours of constant toroidal field $(0, B_y, 0)$. The field lines of the toroidal field run perpendicular to the plane of the paper and point away from the observer. Poloidal and toroidal field peak in the induction region to a value of 10.0 (18 mT for solar values). The left frame in the lower row represents the flow pattern of the poloidal velocity field $(u_x, 0, u_z)$; the arrows indicate the direction of the flow while their length is proportional to the flow velocity. The maximum value of the poloidal flow velocity is 4.1 (about 2 m s^{-1} for solar parameters).

One can see a four-cell structure of the flow: Fluid is streaming vertically (mainly upwards) in the vicinity of the axis of symmetry and transports magnetic flux out of the induction region to the upper (and lower) parts. There the flow turns and material streams back horizontally. In a steady state (such as the picture shows) flux production, transport and dissipation are in balance and the pattern of flow and magnetic field remains constant in time. The preference of the upward flow is due to buoyancy; it is the more marked the more scale heights we use. Lines of constant toroidal velocity are shown in the middle frame of the lower row. It represents a shear flow with the axis of symmetry as the neutral line. The toroidal field produced by this shear has (according to Lenz's rule) the opposite direction of the toroidal field due to the α-effect. The maximum toroidal velocity is 2.05 (about 1 m s^{-1}). Lines of constant density perturbation (deviation from the hydrostatic stratification) are drawn in the right frame of the lower row. Density is reduced with respect to the non-magnetic stratification in the vicinity of the induction strip (leading to buoyancy) and increased in the upper and lower parts. Due to the small value of Γ (as compared to the solar value) the density reduction is quite large (up to 20% of the hydrostatic density) but this does not affect the buoyancy force which depends on G.

Moreover, the density reduction is never big enough to cause an instability of the Rayleigh-Taylor type. Using solar values we can calculate the total magnetic and kinetic energy per unit length in y-direction by integration over the surface of the rectangle. The values are

$$E_{kin}/l = 0.226\ 10^{17}\ \text{Ws m}^{-1}; \quad E_{mag}/l = 0.735\ 10^{18}\ \text{Ws m}^{-1}.$$

The ratio of the energies is $E_{kin}/E_{mag} = 0.0308$; a kinetic energy of only 3% of the magnetic energy is sufficient to limit the growth of the magnetic field. This arises from the fact that the velocity field mainly has the function of transporting the flux out of the induction region to the outer parts where it can be dissipated. From E_{kin} and E_{mag} we may derive mean values of 7 mT for the

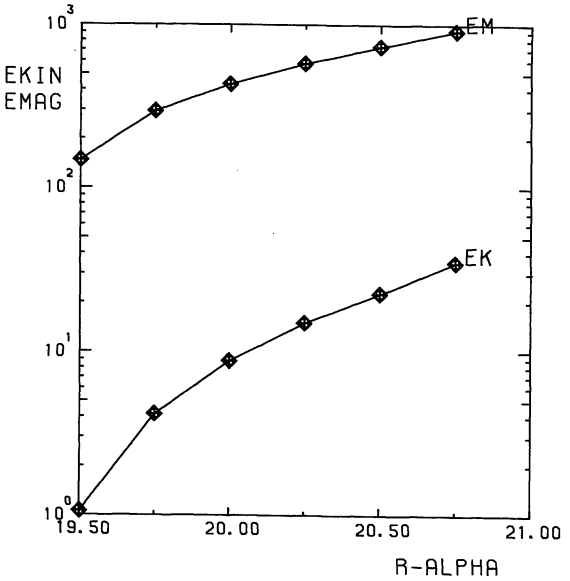

Fig. 4. E_{kin} and E_{mag} (per unit length, arbitrary units) as functions of the dynamo excitation, represented by the magnetic Reynolds number R_α. The critical value is $R_{\alpha,krit} \approx 19.25$. Rhombs indicate the values calculated. (Turbulent case)

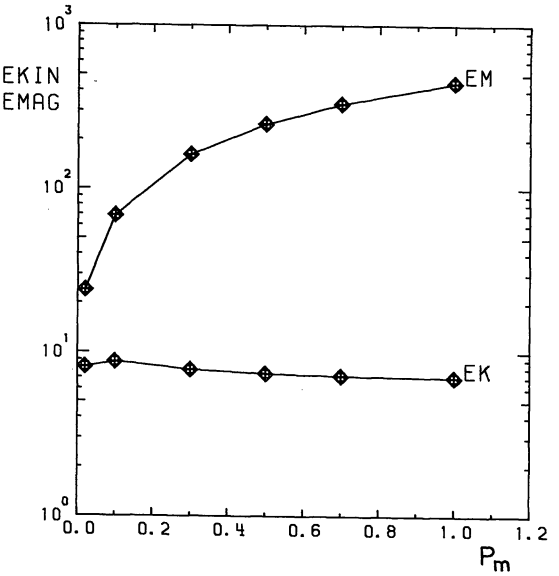

Fig. 5. Dependence of E_{kin} and E_{mag} (per unit length, arbitrary units) on viscosity [$P_m(0)$] for the turbulent case using the same model as in Fig. 1. $P_m(0)=1$ means that turbulent viscosity and turbulent magnetic diffusivity have the same numerical value

magnetic field and 0.2 ms^{-1} for the velocity, compared to peak values of 18 mT and 2 ms^{-1}. Hence, we can infer that the kinetic energy is distributed less uniformly than the magnetic energy.

The case of constant dynamical viscosity ν (non-turbulent case) leads to very similar magnetic field and flow patterns. Due to the increase of the kinematical viscosity ν/ρ with decreasing density, the preference of the upward (buoyant) motion is not as marked as in Fig. 1. The reduced efficiency of buoyancy is visible in the energies, too: the magnetic energy is increased by a factor 6 compared to the case with turbulent viscosity while the kinetic energy is slightly reduced. Hence, reduced buoyancy leads to less effective field amplitude limitation. Increased buoyancy, on the other hand, supports the limitation process. This is shown in Fig. 2 (a, b) which gives the dependence of kinetic and magnetic energy (in arbitrary units) on the number of scale heights of pressure and density. Figure 2a shows the case of turbulent viscosity, Fig. 2b the case of non-turbulent viscosity. It is clearly visible that the kinetic energy behaves similarly in both cases; the magnetic energy in the turbulent case falls significantly with increasing number of scale heights (i.e. increasing buoyancy) while it stays nearly constant in the non-turbulent case. The effect of buoyancy is far more pronounced for turbulent viscosity. From the model of Baker and Temesváry (1966) follows that the isothermal model is sufficient up to 8000 km below the solar photosphere. From the bottom of the convection zone to this point we cover ≈ 10 pressure scale heights and ≈ 6 density scale heights. We can extrapolate the curves given in Fig. 2 to get values relevant for the solar convection zone. In both cases we have a finite amplitude for magnetic field and large scale flow even for 10 scale heights. Buoyancy influences the amplitude of the steady-state field but seems not to be able to suppress dynamo action altogether or to increase the critical value of R_α. We do not give the exact numbers arising from this extrapolation because R_α has to be adjusted anyhow to give the right order of magnitude of the field. Exact values of the amplification parameters for the solar dynamo are still not known.

The time evolution of kinetic and magnetic energy for the model of Fig. 1 is given in Fig. 3. The amplification parameter R_α has been reduced to a slightly supercritical value, i.e. $R_\alpha = 19.5$, in order to slow down the approach of the solution to a steady state. The time is given in units of the magnetic diffusion time $\tau_D = L^2 \cdot \eta^{-1} \approx 10$ yr. Due to the strong damping effects (magnetic diffusivity, turbulent viscosity) the stationary state is reached by a monotonic increase of E_{mag} and E_{kin} and not in an oscillatory manner (Hellmich, 1978) after $\approx 5\tau_D$. The energies of the stationary state as functions of R_α for the same model are given in Fig. 4. We see a fast growth with R_α while E_{kin} grows even slightly faster than E_{mag}, although for $R_\alpha = 20.75$ it is only a few percent of E_{mag}. For $R_\alpha \gtrsim 21.0$ the flow velocity exceeds the value tolerable by the numerical method and further calculations could not be carried out. Figure 5 represents the dependence of the energies on viscosity (P_m) for the turbulent case. Increasing viscosity reduces the efficiency of field limitation substantially as one can see by the growth of the magnetic energy while the kinetic energy stays nearly constant. As the flow is hampered by the strong viscous forces, field limitation occurs at a higher level of E_{mag}. Viscous energy dissipation does not balance this effect. Note that the ratio E_{kin}/E_{mag} grows in the limit $P_m \to 0$. The figures corresponding to Figs. 3–5 for the non-turbulent case show the same qualitative behaviour as those shown for constant kinematical viscosity (turbulent case).

$\alpha\omega$-dynamo

Most of the dynamo models of the solar cycle are of the $\alpha\omega$-type, i.e. the toroidal magnetic field is generated from the poloidal field by means of differential rotation ('ω') while turbulent induction ('α') produces poloidal field out of toroidal field and closes the chain. Differential rotation is observable at the surface of the Sun and as the $\alpha\omega$-models describe many global features of the solar cycle correctly, it seems to be natural to investigate field limitation by large scale velocities for such a dynamo model.

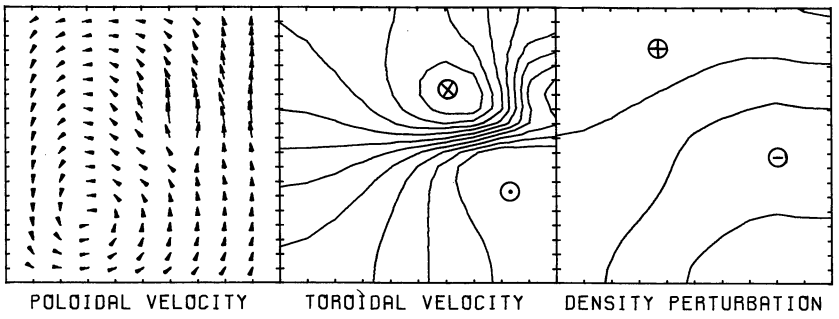

Fig. 6a. Flow pattern and density perturbation for an oscillatory $\alpha\omega$-dynamo [$\Gamma=100$, $G=4$, $P_m(0)=1$, turbulent case, $z_0=0.5$, $z_1=0.45$, $z_2=0.55$, $d=D=0.05$, $R_\alpha=10$, $R_\omega=245$). These patterns do not vary significantly in the course of the cycle, therefore they are only given once. The phase refers to Fig. 6b

This has been done by Nelle (1977) for the incompressible case and we shall give results of calculations with our compressible stratified model. As for the α^2-dynamos we restrict the turbulent induction to a narrow horizontal strip within the integration domain in order to give buoyancy the best opportunity to inhibit dynamo action. We specify the additional vertical toroidal shear du_s/dz introduced in Eq. (6) to have a Gaussian profile:

$$du_s/dz = -\frac{k_0}{D\cdot\sqrt{\pi}}\exp\{-[(z-z_0)/D]^2\}, \tag{18}$$

(18) describes a toroidal flow with a transition from a region of high velocity $z\lesssim z_0$ to a region of low velocity $z\gtrsim z_0$ and a transition region $z_0-D\lesssim z\lesssim z_0+D$. A model with negative vertical shear is necessary to describe the equatorward migration of the spot zone in the course of the solar cycle (Stix, 1976b). k_0 is a constant number which gives the amount of shearing; the Reynolds number $R_\omega=k_0L\eta^{-1}$ measures the inductive effect of the shear flow. The α-effect is assumed to be given by (17). If we take into account the observational evidence that the mean toroidal field is much larger than the mean poloidal field in the solar convection zone, we can assume the field generation due to the α-effect to be small compared to the field generation by shear flow. Therefore we can neglect the term with α in (6). The shear flow is assumed to be constant in time and to be unchanged by the magnetic field. This can be justified by comparing the huge energy content of the solar differential rotation to that of the magnetic fields. Excitation of the $\alpha\omega$-dynamo is controlled by the dynamo number $P=R_\alpha\cdot R_\omega$ with $R_\alpha\ll R_\omega$. We show results for a model with α-effect in the region $0.45\lesssim z\lesssim 0.55$ and a transition zone $D=0.05$. The dynamo is excited for $P\gtrsim P_{\text{crit}}\approx 2300$ (results of linear calculations without Lorentz force). Figure 6a shows the flow pattern and the density perturbation. In the course of the cycle these do not vary significantly; for this reason we show them only once. Figure 6a refers to the phase of the magnetic field shown in Fig. 6b. The parameters are $P=2450$ ($R_\alpha=10.0$, $R_\omega=245.0$), $\Gamma=100.0$, $G=4$ and the turbulent case with $P_m(0)=1$.

The poloidal flow consists mainly of a one-cell structure transporting flux out of the region of maximum magnetic field. There, we find the maximum upward velocities; this region moves slightly towards $x=1$ (equatorwards) as the cycle proceeds. The flow at $z=1$ ('surface') is directed towards $x=0$ ('pole') through the whole cycle. Toroidal flow (the additional shear flow is subtracted) and density perturbation do not change significantly during the cycle; the toroidal flow represents a shear flow which – according to Lenz's rule – opposes the shear of the driving flow $u_s(z)$. Hence, the shear surface is situated in the same region as that of u_s. The density perturbation is negative in the region of maximum magnetic field due to the outflow of material when the field increases. For this model the maximum poloidal velocity is 12.15 (6 m s^{-1}), the maximum toroidal velocity is 6.4 (3.2 m s^{-1}) (values in brackets refer to solar parameters). Thus flow velocities of the order of meters per second (the average values are much smaller) are sufficient to limit the magnetic field produced by an $\alpha\omega$-dynamo to the observed solar value. The velocity field represents a very slow circulation which seems unlikely to be detected under the noise of convective motions in the upper parts of the solar convection zone. This picture does not change significantly if we use a detailed convection zone model instead of the isothermal approximation presented here or change other parameters like $d, D, P_m(0)$, etc. The peak velocities are always of the order of a few meters per second while the average motion is as slow as a few tens of centimeters per second.

Figure 6 (b–g) shows a sequence of magnetic field configurations covering nearly a half period of the oscillation. The period is $0.03\,\tau_D$, a very small value which is caused by the spatial coincidence of shear zone and turbulent induction zone. Spatial separation of the induction effects leads to increasing periods and values comparable to the solar cycle ($\tau\approx 2\cdot\tau_D$) are possible (Deinzer and Stix, 1971). The period is not influenced by the non-linearity introduced in the equations. Dynamo waves of poloidal and toroidal magnetic field travelling in the positive x-direction (from 'pole' to 'equator') are shown in Fig. 6. Nearly half the period is covered in Fig. 6g and the magnetic field polarity is reversed as compared to Fig. 6b. For the velocity field, however, a whole period is covered since the Lorentz force driving the flow is quadratic in B. The equatorward migration of the region of maximum toroidal field leads to the migration of the sunspot zones and the formation of the butterfly diagram. The maximum toroidal field amounts to 5.93 (about 10 mT for solar parameters) while the maximum poloidal field is about 1 mT. The ratio of toroidal to poloidal field depends on R_α/R_ω which can be adjusted to give any desired value (at the present stage of knowledge about the solar convection zone).

4. Conclusions

The results of the calculations can be summarized as follows:

a) The non-linear magnetic field limitation due to large scale circulation works for a compressible stratified medium as well as for an incompressible medium.

b) Buoyancy supports field limitation and (in the case of turbulent viscosity) leads to a much smaller amplitude of the magnetic field as compared to non-buoyant models. However, in every realistic case *buoyancy is not able to inhibit dynamo action totally* or to increase the critical Reynolds number considerably.

c) The geometry of the magnetic field does not differ considerably from that of the linear case. The period of the $\alpha\omega$-dynamo is unchanged.

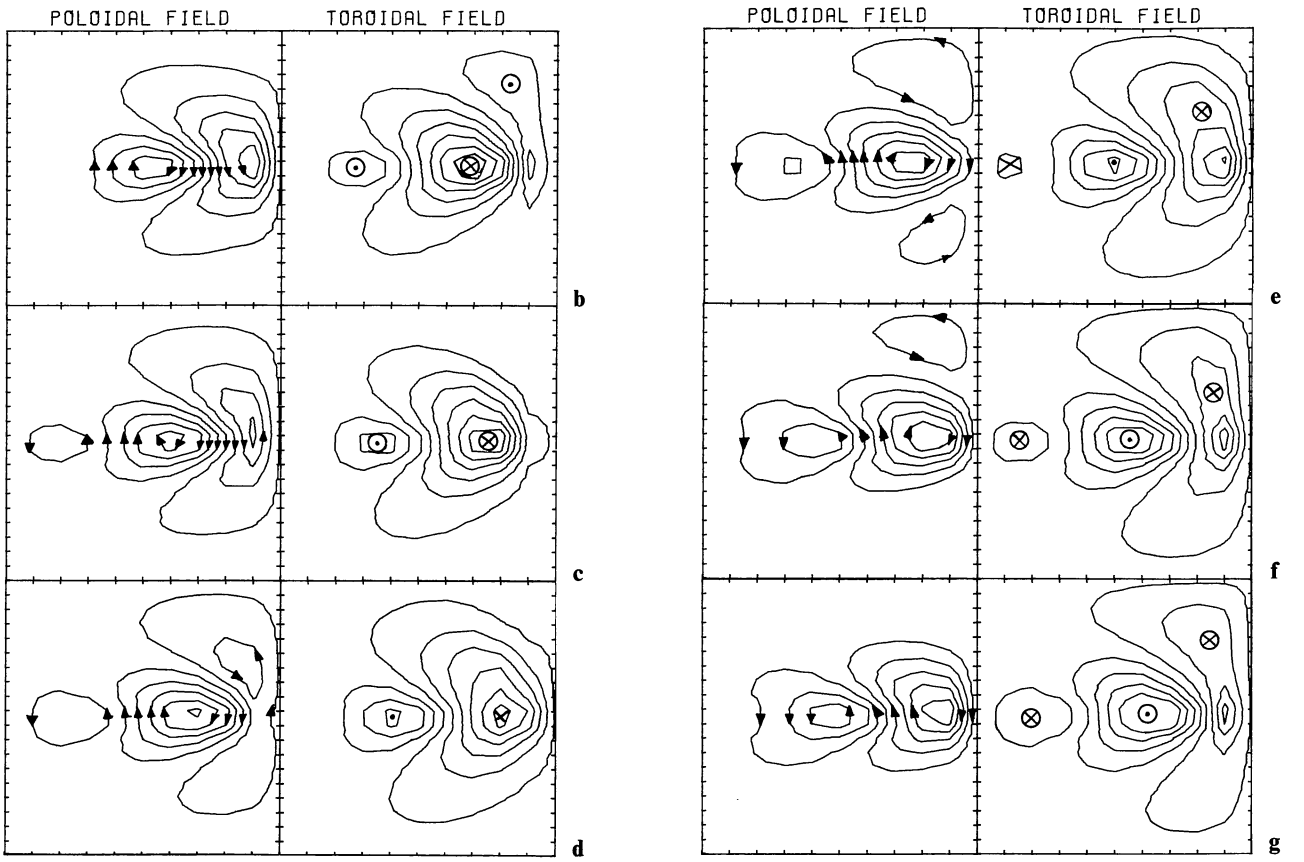

Fig. 6b–g. Series of magnetic field configurations covering nearly a half period of the oscillation. The period is $\tau \approx 0.03\ \tau_D$. The phases are: **b)** $t=0$, **c)** $t \approx 0.1\ \tau$, **d)** $t \approx 0.2\ \tau$, **e)** $t \approx 0.3\ \tau$, **f)** $t \approx 0.4\ \tau$, **g)** $t \approx 0.5\ \tau$

d) Flow velocities of a few meters per second (peak value) may be sufficient to limit the magnetic field to 10 mT (average toroidal field of the Sun). The 'surface' flow of the $\alpha\omega$-dynamo is poleward; this might contribute to the observed poleward migration of the prominence region (Hyder, 1965). The toroidal flow is a shear flow with opposite shearing as compared to the driving shear flow (differential rotation).

e) Usage of a turbulent (constant kinematical) viscosity leads to a larger influence of buoyancy than does non-turbulent (constant dynamical) viscosity. This results from the fact that in the latter case the kinematical viscosity increases with decreasing density. In both cases increased viscosity leads to increased magnetic field amplitude.

The weak points of the models presented here are:

a) Idealized geometry: Although topological equivalent to a spherical shell, a rectangular region does not account for effects of curvature. However, this is not likely to influence the solutions significantly. More restrictive is the fact that the calculations are only two-dimensional. The existence of the solar sector structure and of active lengths prove the necessity of three-dimensional models.

b) Arbitrary spatial distribution of induction effects (α-effect, shear flow) results from our unsufficient knowledge about convection and the solar interior. Calculations with different parameter values produced results that agree to order of magnitude.

c) Besides the spatial distribution also the efficiency of the α-effect is unknown. The amplification factors had to be adjusted to the observed magnetic field strength. However, the flow velocity corresponding to this value seems to be reasonable.

d) The uppermost layers (down to a depth of 10,000 km) of the solar convection zone are not included since they contain too many scale heights to be tolerated by the numerical scheme.

e) Large scale flows like supergranulation and giant cells have been omitted in order to leave the model easy to survey. Supergranulation probably has a vertical extent of about 10,000 km down from the photosphere, a region not covered by the calculations (see d).

f) As we deal with mean field models the effect of fluctuations (sunspots, flux tubes etc,) are not included. However, the rising velocity of individual flux tubes agrees to order of magnitude to the flow velocities obtained in these calculations (Schüßler, 1977; 1978).

Acknowledgements. The author is indebted to Prof. W. Deinzer and Dr M. Stix for valuable discussions. The numerical calculations were carried out with the Univac 1108 of the Gesellschaft für wissenschaftliche Datenverarbeitung mbH, Göttingen.

References

Baker, N., Temesváry, S.: 1966, Tables of convective stellar envelopes, NASA, New York

Busse, F. H.: 1973, *J. Fluid Mech.* **57**, 529

Busse, F. H.: 1975, *J. Fluid Mech.* **72**, 67
Deinzer, W., Stix, M.: 1971, *Astron. Astrophys.* **12**, 111
Deinzer, W., v. Kusserow, U., Stix, M.: 1974, *Astron. Astrophys.* **36**, 6
Dufort, E. C., Frankel, S. P.: 1953, *Math. Tab. and Other Aids to Comp.* **7**, 135
Frisch, U., Pouquet, A., Léorat, J., Mazure, A.: 1975, *J. Fluid Mech.* **68**, 769
Galloway, D. J., Proctor, M. R. E., Weiss, N. O.: 1977, *Nature* **266**, 686
Gubbins, D.: 1975, *Geophys. J. Roy. Astron. Soc.* **42**, 295
Hellmich, R.: 1978, *Geophys. Astrophys. Fluid Dyn.* **10**, 89
Hyder, C. L.: 1965, *Astrophys. J.* **141**, 272
Köhler, H.: 1973, *Astron. Astrophys.* **25**, 467
Krause, F.: 1976, in *Basic Mechanisms of Solar Activity*, Proc. IAU-Symp. 71, ed. by Bumba, V., Kleczek, J., Dordrecht/Boston
Malkus, W. V. R., Proctor, M. R. E.: 1975, *J. Fluid Mech.* **67**, 417
Moffat, H. K.: 1972, *J. Fluid Mech.* **53**, 385
Moffat, H. K.: 1978, Magnetic field generation in electrically conducting fluids, Cambridge University Press, Cambridge
Nelle, K.: 1977, Diplomarbeit, Universität Göttingen
Pähler, A.: 1976, Diplomarbeit, Universität Göttingen
Parker, E. N.: 1975, *Astrophys. J.* **198**, 205
Parker, E. N.: 1977, *Astrophys. J.* **215**, 370
Peckover, R. S., Weiss, N. O.: *Monthly Notices Roy. Astron. Soc.* **182**, 189
Proctor, M. R. E.: 1977, *J. Fluid Mech.* **80**, 769
Pouquet, A., Patterson, G. S.: 1978, *J. Fluid Mech.* **85**, 305
Roberts, P. H., Stix, M.: 1972, *Astron. Astrophys.* **18**, 453
Rüdiger, G.: 1973, *Astron. Nachr.* **294**, 183
Schüßler, M.: 1975, *Astron. Astrophys.* **38**, 263
Schüßler, M.: 1977, *Astron. Astrophys.* **56**, 439
Schüßler, M.: 1979, *Astron. Astrophys.* **71**, 79
Soward, A. M.: 1973, *Phil. Trans. Roy. Soc. London* A **275**, 611
Steenbeck, M., Krause, F.: 1969, *Astron. Nachr.* **291**, 271
Stix, M.: 1972, *Astron. Astrophys.* **20**, 9
Stix, M.: 1975, *Astron. Astrophys.* **42**, 85
Stix, M.: 1976a, in *Basic Mechanisms of Solar Activity*, Proc. IAU-Symp. 71, ed. by. Bumba, V., Kleczek, J., Dordrecht/Boston
Stix, M.: 1976b, *Astron. Astrophys.* **47**, 243
Vainshtein, S. I.: 1971, *Soviet Physics* JETP **34**, 327
Watanabe, H.: 1977, *J. Geomagn. Geoelectr.* **29**, 191
Yoshimura, H.: 1978a, *Astrophys. J.* **220**, 692
Yoshimura, H.: 1978b, *Astrophys. J.* **221**, 1088

Note added in proof: Recent statistical analysis of intrinsic motions of sunspots in latitude for the period 1954–1964 (Balthasar, 1978; private communication) show the preference of a mean poleward velocity of 0.03 °/d$\approx$0.4 m s^{-1} in the vicinity of the equator which compares nicely with the velocities found in this paper for the poleward surface flow due to the dynamo (Fig. 6a).